Numerical study of a morphology diagram in the large undercooling limit using a phase-field model

Raz Kupferman, Ofer Shochet, and Eshel Ben-Jacob
School of Physics and Astronomy, Raymond and Beverly Sackler Faculty of Exact Sciences, Tel Aviv University, Tel Aviv 69978, Israel
(Received 31 August 1993)

We present a numerical study of asymptotic late-stage growth in a phase-field model. After a long transient time the patterns are independent of initial conditions, and have a well-defined shape-preserving envelope which propagates at constant velocity. To distinguish between implicit and explicit anisotropies, a model with explicit fourfold anisotropy is solved on a triangular lattice. Distinct morphologies are observed, characterized by the envelope shape and by their constituent growth elements (dendrites, parity-broken dendrites, or tip-splitting fingers).

PACS number(s): 64.60.−i, 05.70.Ln, 64.70.Dv, 02.70.Rw

During the last decade, a successful approach in the study of diffusive patterning was to focus on the formation of isolated growth elements (e.g., dendrites, fingers, and bubbles) (see Refs. [1–5] and references therein). This approach was motivated by the idea that many of the most important features of pattern formation can still be understood while ignoring the full time-dependent growth of the entire structure (the morphology). This strategy led to the discovery of the singular nature of microscopic interfacial dynamics, and to the formulation of solvability criteria for the existence of different types of isolated growth elements [6].

Focusing on isolated elements is a reasonable approximation for the case of low undercooling, where the global average density of the growing phase is small. However, in general, and in particular at large undercooling, the observed structures are much more complex [7–11], and interactions between branches cannot be ignored. In this case, it is necessary to consider the global morphology resulting from the self-organization of the various growth elements. On a larger scale, this self-organization forms a well-defined envelope. Recent numerical simulations [12] indicate that this envelope is shape preserving and grows at constant rate. The shape of this envelope is correlated to the internal structure, thus can be used as a simple characterization to distinguish between various morphologies. Moreover, different morphologies exhibit different functional dependencies of the growth velocity on the parameters. Under certain conditions, different morphologies can coexist for the same control parameters [13]. The transition between morphologies is sharp, and accompanied with a discontinuity of the slope of the velocity plot at the transition. These findings suggest the existence of a morphology determination principle.

Clearly, the interplay between growth elements and the morphology requires a study of late-stage growth of very decorated patterns. At present, all the information on morphology properties is for algorithmic models which are characterized by strong noise, whereas most of our understanding of the formation of growth elements is with respect to noiseless differential equations. It is necessary to adopt a model tractable for the study of both growth elements and global structures. In this paper we employ the phase-field model [14,15] for the performance of large scale numerical simulations, and for a study of morphology diagrams in the large undercooling limit. On the one hand, such numerical procedure incorporates much weaker noise than any algorithmic model. On the other hand, the phase-field model reduces asymptotically to the free boundary model for which analytic solutions for growth elements exist.

We take here the familiar form of the phase-field model defined by the dimensionless equations

$$\epsilon^2 \frac{\partial \phi}{\partial t} = \epsilon^2 \nabla^2 \phi + f(\phi, u), \tag{1}$$

and

$$\frac{\partial u}{\partial t} = \nabla^2 u + \frac{\partial \phi}{\partial t}, \tag{2}$$

where ϕ is the order parameter, u is the dimensionless temperature subject to the boundary condition $u(\infty) = -\Delta$, and Δ is the dimensionless undercooling. Lengths are measured in units of the characteristic diffusion length ℓ, whereas time is measured in units of ℓ^2/D, D being the heat diffusion coefficient of the substance. The function $f(\phi, u)$ is the "driving force" of the phase transition, derived from the homogeneous part of the free energy. We adopt the form proposed by Kobayashi [16],

$$f(\phi, u) = \phi(1-\phi)\left(\phi - \frac{1}{2} - \epsilon \tanh \lambda u\right), \tag{3}$$

which is derived from a double-well shaped potential with minima at $\phi = 0$ (liquid) and $\phi = 1$ (solid). This functional form has numerical advantages. First, the fact that the equilibrium values of the phases remain constant for all values of u saves computing time, as ϕ is stationary in most of the space. Second, the strong nonlinear de-

pendence of the potential-tilt function $\tanh(\lambda u)$ (in all our simulations $5 \leq \lambda\Delta \leq 10$) ensures a rapid solidification rate even when the interfacial temperature is close to equilibrium. These two advantages enabled the execution of large scale simulations required for studies of late-stage growth.

The parameter ϵ is the characteristic thickness (in dimensionless units) of the domain wall connecting the solid phase to the liquid phase at equilibrium ($u = 0$). Since ϵ is the ratio of a mesoscopic scale (the thickness of the interface) and a macroscopic scale (decay length of the temperature field), it is often considered as a mathematical entity used for taking the limit $\epsilon \to 0$. In this limit, the phase-field model reduces to the free boundary model [17,18], with the boundary condition for the temperature at the interface, u_i, given by

$$u_i = -\frac{1}{\lambda}\tanh^{-1}\frac{\sqrt{2}}{2}(\kappa + v_n), \tag{4}$$

where κ is the local curvature of the interface, and v_n is its velocity in the normal direction. This boundary condition is a generalization of the familiar Gibbs-Thompson (surface tension) and surface kinetic corrections, $u_i = -d_0\kappa - \beta_0 v_n$ [19].

A rigorous way to include anisotropy is to derive the Landau free energy from an anisotropic interaction, as proposed by Caginalp and Fife [20]. Introduction of fourfold anisotropy implies the replacement of the Laplacian operator in Eq. (1) by the fourth order operator

$$\epsilon^2\nabla^2 \longrightarrow -\frac{3}{4}\eta\epsilon^4\left(\frac{\partial^4\phi}{\partial x^4} - 6\frac{\partial^4\phi}{\partial x^2\partial y^2} + \frac{\partial^4\phi}{\partial y^4}\right) + \epsilon^2\nabla^2, \tag{5}$$

the parameter η controlling the level of anisotropy. In the free boundary limit, this modification affects only the interfacial temperature, now given by

$$u_i = -\frac{1}{\lambda}\tanh^{-1}\frac{\sqrt{2}}{2}\{[\gamma(\theta) + \gamma''(\theta)]\kappa + \delta(\theta)v_n\}, \tag{6}$$

where

$$\gamma(\theta) \approx 1 + \frac{\eta}{80}\cos 4\theta, \qquad \delta(\theta) \approx 1 + \frac{3\eta}{80}\cos 4\theta, \tag{7}$$

and θ is the angle between the normal to the interface and the x axis.

A distinction between the implicit anisotropy of the underlying computational grid and the explicit anisotropy of the model is necessary for investigating numerically the zero-anisotropy limit [21]. To this end, Eqs. (1) and (2) were solved numerically on a triangular lattice, thus creating a distinction between the six preferred orientations of the lattice, and the four preferred orientations of the model. The time evolution was integrated using an explicit scheme. The size of the system was up to 2500×2800 grid points. Such a large system is required to satisfy the following cascade of lengths: (grid size) < (decay length of ϕ) < (decay length of u) < (width of a growth element) $\ll$ (overall structure). Typical well-developed structures required up to 10 CPU hours on a Cray YMP for vectorized code.

The results presented here are for an open geometry with $\epsilon = 0.2$, $\lambda = 10$, $\Delta = 0.5 - 1.0$, and $\eta = 0.0 - 0.5$. The initial conditions consist of a solid nucleus ($\phi = 1$) at equilibrium temperature ($u = 0$), surrounded by undercooled liquid ($\phi = 0$ and $u = -\Delta$). The shape of the nucleus is a circle weakly perturbed with a superposition of harmonics. In the following figures, the boundaries of the solid domains are $\phi = \frac{1}{2}$ contour lines.

The first issue is to provide a characterization of asymptotic late-stage growth. A time sequence of four solid contours is shown for an isotropic system ($\eta = 0$) in Fig. 1. The mark of the initial perturbation is clearly visible in patterns *a* and *b*, fading out in pattern *d*, where the structure forms a circular envelope which then remains shape preserving. This behavior repeated itself for all the initial conditions that we have checked.

Figure 2 shows a similar sequence of solid contours for dendritic growth, where the growing structure forms a diamondlike shape-preserving envelope. A more rigorous definition of the envelope can be provided using a contour line of the temperature field. Such contour lines surround the entire structure close to the tips of the propagating solid. A second possibility is to define the envelope using an ensemble average of different growth realizations (differing in their initial conditions), as was done by Shochet *et al.* [12]. In our case such a procedure is numerically impractical. Instead we note that, for shape-preserving growth, ensemble averaging is equivalent to time averaging over a rescaled system. To show that, we plot in Fig. 3(a) superimposed solid contours. These contours are rescaled in space $\phi = \phi(\vec{x}/R_{\max}(t))$, where $R_{\max}(t)$ is the maximum distance of a solid point to the center of the initial nucleus. A shape-preserving envelope is constructed, forming a smooth shape as $t \to \infty$.

Another criterion for asymptotic late-stage growth can be defined by the following dynamical quantities: (1) the maximum radius of the pattern, $R_{\max}(t)$, and (2) the solid fraction, $\rho(t)$. The latter is calculated by dividing the total surface integral of ϕ by the area of a circle with

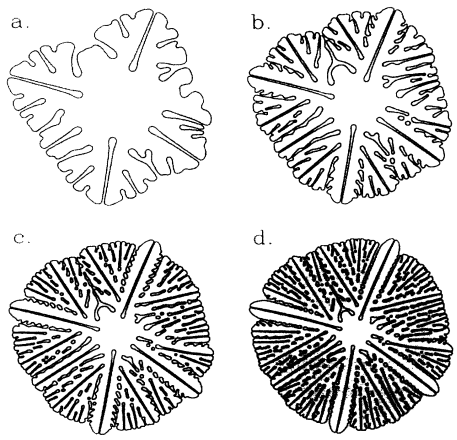

FIG. 1. A time sequence of solid contours for $\Delta = 0.8$ and $\eta = 0$. The average velocity of propagation of the front is 0.8. The contours correspond to growth time of (a) $t = 120$, (b) $t = 180$, (c) $t = 240$, and (d) $t = 300$.

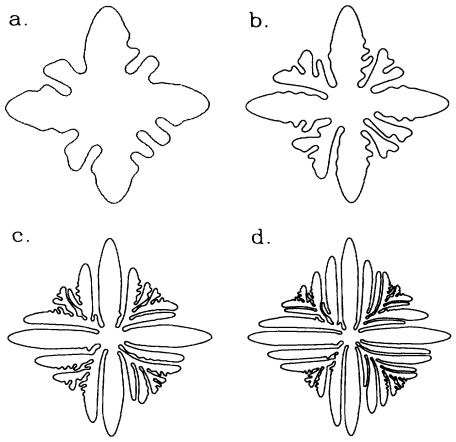

FIG. 2. A time sequence of solid contours for $\Delta = 0.7$ and $\eta = 0.3$. The average velocity of propagation of the front is 0.41. The contours correspond to growth time of (a) $t = 120$, (b) $t = 240$, (c) $t = 480$, and (d) $t = 720$.

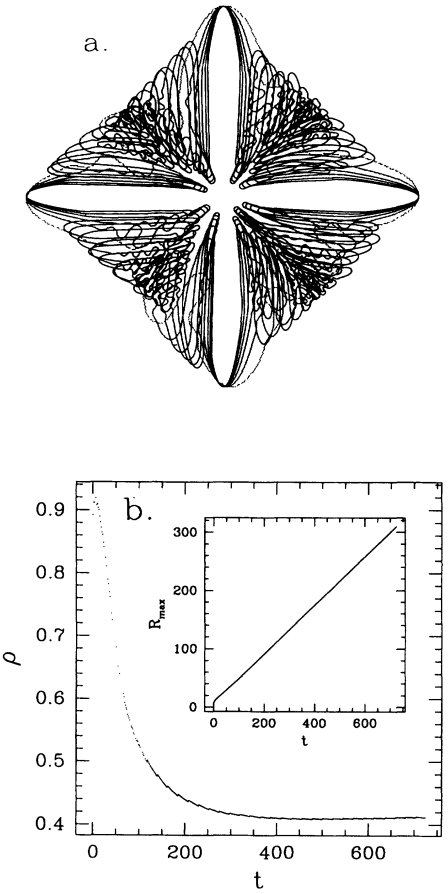

FIG. 3. (a) Superimposed contours of the rescaled solid-liquid interface, $\phi(\vec{x}/R_{\max}) = \frac{1}{2}$, for $\Delta = 0.7$ and $\eta = 0.3$. The time interval between two consecutive contours is $\Delta t = 120$. (b) The average solid fraction ρ and the maximum distance of a solid point to the center, $R_{\max}$, versus time.

radius $R_{\max}(t)$. The asymptotic regime is attained when both $\bar{v}(t) = \dot{R}_{\max}(t)$ and $\rho(t)$ reach asymptotic values [Fig. 3(b)]. For isotropic systems (and therefore circular envelopes), the asymptotic solid fraction ρ_∞ is equal to the undercooling Δ [12,22]. For anisotropic growth (fourfold in our case), $\rho_\infty < \frac{2}{\pi}\Delta$ for a concave envelope and $\rho_\infty > \frac{2}{\pi}\Delta$ for a convex envelope. Hence ρ_∞ provides a simple measure for the shape of the envelope.

Next, we turn to the description of the morphology diagram presented in Fig. 4. From the point of view of individual growth elements, four patterns are identified. Compact growth is obtained for very high undercooling ($\Delta \gtrsim 0.9$). In this regime, growth is characterized by a compact solid filled with liquid droplets. From energetical considerations, steady-state compact patterns are impossible for $\Delta < 1$. Therefore steady propagation of a compact front implies solid-liquid decomposition behind the front. This solution can be calculated analytically by considering a one-dimensional system, where the holes are reflected as periodic oscillations of the phase [23].

The second pattern is the dendrite. Ordinary dendrites have parabolic shapes with a train of sidebranches shooting out. Here, at relatively low undercooling, the dendrites develop weak undulations rather than decorated sidebranches. At higher undercooling, the dendrites are densely packed, so that each dendrite is parabolic only close to the tip which is connected to a straight trunk.

The third pattern is tip-splitting fingers, which are obtained for low undercooling and weak anisotropy. The fourth pattern is a parity-broken dendrite which has recently been identified and studied by Ihle and Müller-Krumbhaar [21,24] (referred to as parity-broken fingers).

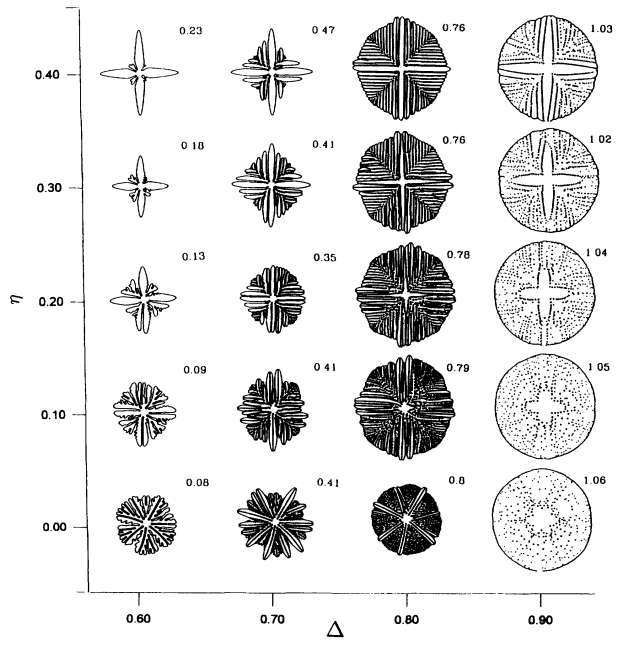

FIG. 4. Morphology diagram for Δ=0.6–0.9 and η =0.0-0.4. The asymptotic velocity of the envelope appears at the upper-right corner of each pattern.

In a forthcoming publication [25], we will show that this growth element is a steady-state solution of the system *in addition* to the dendritic one. In our simulations parity-broken dendrites are obtained even for isotropic conditions.

Next, we consider the global structures and the envelope shapes. In the isotropic limit, both for tip-splitting fingers (dense-branching morphology) and for parity-broken dendrites, the envelope is circular. For very large undercooling, where the morphology becomes compact, the envelope and the liquid droplet ordering show a weak sixfold symmetry. In the presence of anisotropy the envelope becomes fourfold symmetric. For low undercooling, the envelope is concave and the growth elements are dendrites. In Ref. [12], the space between the four main trunks is filled with sidebranches emanating perpendicularly from the main trunks. Here, this space is filled with dendrites parallel to the main trunks, which are emitted from oscillating fingers growing in the 45° directions. For higher undercooling, the envelope is a convex fourfold symmetric octagon, formed by a similar process of tip splitting in the 45° directions. During each splitting, two parity-broken dendrites are emitted to the 0° and 90° directions.

We note that in the transition from a concave envelope (dendrites) to a convex (parity-broken dendrites) envelope the velocity undergoes a qualitative change. For the concave morphology it is an increasing function of anisotropy, whereas for the convex morphology it is the opposite. The transition between the two regimes seems to occur in the vicinity of the $\Delta = 0.7$ and $\eta = 0.2$ realization, where the envelope is partly concave and partly convex.

To conclude, we showed in this paper the formation of four types of growth elements creating different morphologies via different mechanisms of self-organization. At least three of these growth elements can be identified as steady-state solutions of the model. In addition, the dendritic morphology obtained here exhibits a different ordering compared to other models. Our conjecture is that these results reflect a morphology selection principle. For the same control parameters, various growth elements can grow, and perhaps can order in more than one manner, but only one morphology is dynamically selected. We hope that such numerical studies will provide new insight which will lead in the future to a formulation of a generalized solvability mechanism of growth-element-morphology interplay.

We are grateful to Z. Schuss for his assistance to this study. We have also benefited from useful discussion with A. Bayliss, D. Kessler, H. Levine, and D. Rand. R. K. thanks A. Bayliss for his hospitality at Northwestern University. We thank the Institute for Theoretical Physics and the participants of the Program in "Spatially Extended Non-Equilibrium Systems" for hospitality and discussions. This study was partially supported by a grant from the G.I.F., the German–Israeli Foundation for Scientific Research and Development, by Grant No. 9200051 from the United States–Israel Binational Science Foundation (BSF), and by the Program for Alternative Thinking at Tel-Aviv University.

[1] D.A. Kessler, J. Koplik, and H. Levine, Adv. Phys. **37**, 255 (1988).
[2] J.S. Langer, Science **243**, 1150 (1989).
[3] E. Ben-Jacob and P. Garik, Nature (London) **343**, 523 (1990).
[4] H. Müller-Krumbhaar and W. Kurz, in *Phase Transformation in Materials*, edited by P. Haasen (VCH-Verlag, Weinheim, 1991).
[5] E.A. Brener and V.I. Mel'nikov, Adv. Phys. **40**, 53 (1991).
[6] M. Ben-Amar and Y. Pomeau, Europhys. Lett. **2**, 307 (1986).
[7] P. Oswald, J. Bechhoefer, and F. Melo, Mater. Res. Bull. **16**, 38 (1991).
[8] Á. Buka and N. Éber, Europhys. Lett. **2**, 477 (1993).
[9] E. Ben-Jacob, R. Godbey, N.D. Goldenfeld, J. Koplik, H. Levine, T. Mueller, and L.M. Sander, Phys. Rev. Lett. **55**, 1315 (1985).
[10] D.G. Grier, E. Ben-Jacob, R. Clarke, and L.M. Sander, Phys. Rev. Lett. **56**, 1264 (1986).
[11] Á. Buka, J. Ketesz, and T. Vicsek, Nature (London) **323**, 424 (1986).
[12] O. Shochet, K. Kassner, E. Ben-Jacob, S.G. Lipson, and H. Müller-Krumbhaar, Physica A **181**, 136 (1992); **197**, 87 (1992).
[13] Ofer Shochet and Eshel Ben-Jacob, Phys. Rev. E **48**, 4168 (1993).
[14] J.B. Collins and H. Levine, Phys. Rev. B **31**, 6119 (1985).
[15] J.S. Langer, in *Directions in Condensed Matter Physics*, edited by G. Grinstein and G. Mazenko (World Scientific, Singapore, 1986).
[16] Ryo Kobayashi, Physica D **63**, 410 (1993).
[17] G. Caginalp and P.C. Fife, Phys. Rev. B **33**, 7792 (1986); SIAM J. Appl. Math. **48**, 506 (1986).
[18] Raz Kupferman, O. Shochet, E. Ben-Jacob, and Zeev Schuss, Phys. Rev. B **49**, 16045 (1992).
[19] Raz Kupferman, Ofer Shochet, Eshel Ben-Jacob, and Zeev Schuss (unpublished).
[20] G. Caginalp and P.C. Fife, Phys. Rev. B **34**, 4940 (1986).
[21] T. Ihle and H. Müller-Krumbhaar, Phys. Rev. Lett. **70**, 3083 (1993).
[22] E.A. Brener, H. Müller-Krumbhaar, and D.E. Temkin, Europhys. Lett. **17**, 535 (1992).
[23] M. Zuckerman, Raz Kupferman, O. Shochet, E. Ben-Jacob, and Z. Schuss (unpublished).
[24] E. Brener, H. Müller-Krumbhaar, Y. Saito, and D. Temkin, Phys. Rev. E **47**, 1151 (1993).
[25] R. Kupferman, D.A. Kessler, and E. Ben–Jacob (unpublished).

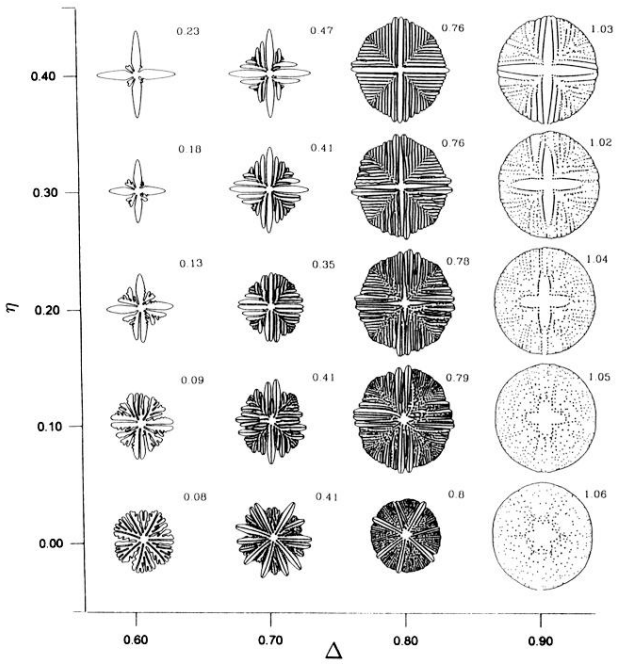

FIG. 4. Morphology diagram for Δ=0.6–0.9 and η =0.0-0.4. The asymptotic velocity of the envelope appears at the upper-right corner of each pattern.